LETTER

doi:10.1038/nature10314

# Decoherence in crystals of quantum molecular magnets

S. Takahashi[1,2,3], I. S. Tupitsyn[4,5], J. van Tol[6], C. C. Beedle[7]†, D. N. Hendrickson[7] & P. C. E. Stamp[4,5]

**Quantum decoherence is a central concept in physics. Applications such as quantum information processing depend on understanding it; there are even fundamental theories proposed that go beyond quantum mechanics[1–3], in which the breakdown of quantum theory would appear as an 'intrinsic' decoherence, mimicking the more familiar environmental decoherence processes[4]. Such applications cannot be optimized, and such theories cannot be tested, until we have a firm handle on ordinary environmental decoherence processes. Here we show that the theory for insulating electronic spin systems can make accurate and testable predictions for environmental decoherence in molecular-based quantum magnets[5]. Experiments on molecular magnets have successfully demonstrated quantum-coherent phenomena[6–8] but the decoherence processes that ultimately limit such behaviour were not well constrained. For molecular magnets, theory predicts three principal contributions to environmental decoherence: from phonons, from nuclear spins and from intermolecular dipolar interactions. We use high magnetic fields on single crystals of $Fe_8$ molecular magnets (in which the Fe ions are surrounded by organic ligands) to suppress dipolar and nuclear-spin decoherence. In these high-field experiments, we find that the decoherence time varies strongly as a function of temperature and magnetic field. The theoretical predictions are fully verified experimentally, and there are no other visible decoherence sources. In these high fields, we obtain a maximum decoherence quality-factor of $1.49 \times 10^6$; our investigation suggests that the environmental decoherence time can be extended up to about 500 microseconds, with a decoherence quality factor of $\sim 6 \times 10^7$, by optimizing the temperature, magnetic field and nuclear isotopic concentrations.**

Environmental decoherence processes are reasonably well understood at the atomic scale[9] (although some poorly understood noisy sources remain[10]). However both quantum information processing, and the fundamental tests noted above, require an understanding of decoherence in larger systems, where experimental decoherence rates are usually much larger than theoretical predictions. This discrepancy is usually attributed to 'extrinsic' sources (external noise, uncontrolled disorder/impurities). We thus need to find systems, with many degrees of freedom, where extrinsic decoherence can be eliminated, and where we have a quantitative understanding of other decoherence sources.

Many insulating electronic spin systems are currently the subject of intense experimental interest, notably in semiconductor quantum dots[11,12], nitrogen-vacancy centres in diamond[13–15] and large-spin magnetic molecules[6–8]. In all these systems, three environmental decoherence mechanisms are involved. The electronic spins couple locally to (1) phonons (an oscillator bath[16]); (2) to large numbers of nuclear spins (a spin bath[17]); and (3) to each other via dipolar interactions. The long range of dipolar interactions is a major problem: it makes quantum error correction more difficult, is theoretically complicated[18] and is very hard to eliminate experimentally.

In these crystalline $Fe_8$ molecular magnets, the electronic spins are structurally ordered, and quantum coherence is observed in the collective (magnon) motion of the spins, rather than in single qubit dynamics. Two great advantages of the $Fe_8$ system[19] are that the interaction strengths are well known, allowing quantitative predictions, and that it can be prepared with little disorder and few impurities, reducing the danger of extrinsic decoherence. The number of relevant environmental degrees of freedom is very large; depending on isotopic concentrations, there are $10^{50}$–$10^{54}$ nuclear spin levels in each molecule, and the system couples to a bulk phonon bath.

In the spin echo experiments described here, a Hahn echo sequence[20] was created in two single crystals of $Fe_8$ molecules, with natural isotopic concentrations, using a 240-GHz pulsed ESR (electron spin resonance) spectrometer[21,22]. Thus a uniform ESR precession mode (a $\mathbf{k} = 0$ magnon, where $\mathbf{k}$ is the wave vector of the magnon) interacts with its surroundings, and we measure the decoherence time $T_2$. At low temperature, each electronic spin system behaves as a two-level quantum bit (qubit), with a splitting $2\Delta_o$ that depends strongly on the local transverse field $\mathbf{H}_\perp$, perpendicular to the easy axis $\hat{z}$ (see Fig. 1 inset). Almost all previous experiments on electron spin systems examined the low-field regime, where nuclear spin decoherence is very strong; here we go to the high-field regime, where its effects are much weaker. Typical ESR results are shown in Fig. 1; we discuss them in detail below.

To understand $T_2$, and the ESR lineshape, we need to look at the processes contributing to them. For convenience, we define a dimensionless decoherence rate $\gamma_\phi = \hbar/\Delta_o T_2$ (where $\hbar$ is Planck's constant $h$ divided by $2\pi$) and the associated 'decoherence $Q$-factor', $Q_\phi = \pi/\gamma_\phi$. Then the processes contributing to $\gamma_\phi$ are as follows (the full quantitative discussion, for the two samples in this experiment, is given in Supplementary Information):

First, nuclear spins interact locally with each molecular spin, and cause decoherence by a 'motional narrowing' process in which they attempt to entangle with the fast-moving qubit[18,23]. The nuclear decoherence rate is $\gamma_\varphi^N = E_o^2/2\Delta_o^2$, where $E_o$ is the half-width of the Gaussian multiplet of nuclear spin states coupled to the qubit; and the nuclear contribution to the ESR linewidth is just $E_o$. Now in this experiment, with naturally occurring isotopic concentrations, $E_o = 4 \times 10^{-4}$ K at these fields, where $\Delta_o = 5.75$ K. Thus $\gamma_\varphi^N \approx 10^{-9}$ is very small, simply because $\Delta_o$ is so large in these fields; and the nuclear spin contribution ($\sim E_o$) to the linewidth is also very small compared to the main contributions. Isotopic substitution of deuterium for the 120 protons in each molecule will further decrease $\gamma_\varphi^N$ by a factor of 15.2 to $\gamma_\varphi^N \approx 7 \times 10^{-11}$. In principle, there can be a 'noise' contribution from the intrinsic nuclear dynamics caused by internuclear interactions[17]; however, in contrast to quantum dot systems[24], such contributions are very small in molecular magnets[23] (even in systems with strongly interacting nuclei like $Mn_{12}$, where they have been seen[25]).

[1]Department of Chemistry, University of Southern California, Los Angeles, California 90089, USA. [2]Institute for Terahertz Science and Technology, University of California, Santa Barbara, California 93106, USA. [3]Department of Physics, University of California, Santa Barbara, California 93106, USA. [4]Pacific Institute of Theoretical Physics, University of British Columbia, Vancouver, British Columbia V6T 1Z1, Canada. [5]Department of Physics and Astronomy, University of British Columbia, Vancouver, British Columbia V6T 1Z1, Canada. [6]National High Magnetic Field Laboratory, Florida State University, Tallahassee, Florida 32310, USA. [7]Department of Chemistry and Biochemistry, University of California, San Diego, La Jolla, California 92093, USA. †Present address: National High Magnetic Field Laboratory, Florida State University, Tallahassee, Florida 32310, USA.

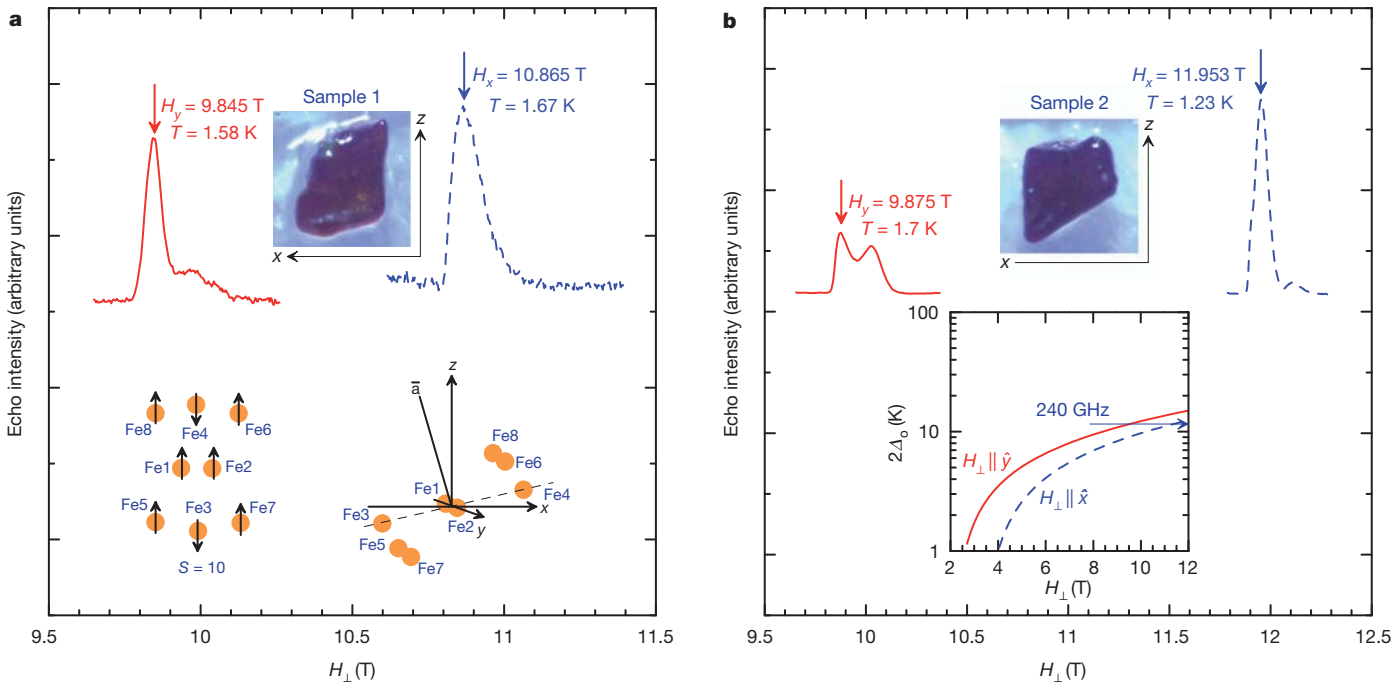


**Figure 1 | Typical ESR spectra, showing echo intensity as a function of transverse magnetic field, $H_\perp$.** Data are shown for two different samples, at different temperatures and orientations of field, and at $\omega_{ESR} = 240$ GHz. **a**, Sample 1. Solid red line, $\mathbf{H}_\perp \| \hat{y}$, $T = 1.58$ K; dashed blue line, $\mathbf{H}_\perp \| \hat{x}$, $T = 1.67$ K. Top inset, sample dimensions are approximately $z$: $x$: $y$ = 1,000: 700: 250 μm. Lower left inset, the low-$T$ spin structure of the $Fe_8$ molecule. Lower right inset, the directions of the easy ($z$), hard ($x$) and intermediate ($y$) axes of an $Fe_8$ molecule (ā approximately gives the direction of the crystallographic vector **a**). **b**, Sample 2. Solid red line, $\mathbf{H}_\perp \| \hat{y}$, $T = 1.7$ K; dashed blue line, $\mathbf{H}_\perp \| \hat{x}$, $T = 1.23$ K. Top inset, sample dimensions are approximately $z$: $x$: $y$ = 900: 800: 400 μm. Bottom inset, tunnelling splitting, $2\Delta_o$, as a function of transverse field at $\mathbf{H}_\perp \| \hat{y}$ (solid red line) and at $\mathbf{H}_\perp \| \hat{x}$ (dashed blue line).

Second, the form of the local spin–phonon interaction is determined by the system symmetry. At high fields this interaction simplifies, and we find a dimensionless phonon decoherence rate[18] given by $\gamma_\varphi^{ph} = \left[\left(\mathcal{F}_{AS}\Delta_o^2\right)/\left(\pi\rho c_s^5\hbar^3\right)\right]\coth(\Delta_o/k_BT)$, where $\rho$ is the sample density, $c_s$ the sound velocity, and $\mathcal{F}_{AS}$ the relevant spin–phonon matrix element. The contribution of this spin-phonon process to the ESR linewidth is negligible.

Third, the intermolecular dipole interaction directly couples the $\mathbf{k} = 0$ ESR precession mode to finite-momentum magnons; it may decay spontaneously into multiple magnons, or scatter off existing thermal magnons. This process affects the ESR lineshape and the decoherence rate very differently. The long-range dipolar interaction creates a distribution of demagnetization fields around the sample. In highly polarized samples, this is strongly sample-shape dependent, but for annealed samples, it is Gaussian distributed[26,27]; in both cases it can be calculated numerically. The lineshape then reflects the quite broad distribution of these fields. However, decoherence comes from the magnon decay process described above, and depends only on the phase space available for these processes at the resonance field; it can then be calculated directly from the analytic expression for this process. At the experimental temperatures, the magnon decoherence rate is $\sim\exp(-2\Delta_o/k_BT)$, where $k_B$ is Boltzmann's constant and $T$ is temperature, coming almost entirely from thermal magnon scattering.

Last, there can be extrinsic contributions from impurities and defects, which typically cause the easy-axis anisotropy parameter $D$ of the $Fe_8$ Hamiltonian to fluctuate around the sample (the '$D$-strain' effect[28,29]). This will then contribute to the ESR linewidth. Such static impurities and defects can cause $\Delta_o$ to vary in the sample (although we find no evidence for such a spread in this experiment). However they can not contribute to decoherence at all, provided they are static, because then they simply shift the individual qubit energies. On the other hand any impurities or defects with significant dynamics will cause extrinsic decoherence.

In Fig. 2 we show how these contributions to the decoherence rate are predicted to vary with field and temperature for a crystalline $Fe_8$ system. The spin-phonon contribution $\gamma_\varphi^{ph}$ increases with applied transverse field, because the available phonon phase space increases sharply with $\Delta_o$. However the nuclear spin decoherence rate decreases with field: roughly $\gamma_\varphi^N \propto 1/\Delta_o^2$, because $E_o$ changes quite slowly with field (and also decreases as $\Delta_o$ increases). Thus there is a crossover, with a minimum $\gamma_\phi \approx 10^{-7}$ when $\Delta_o \approx 1$ K. However these two 'single-qubit' decoherence mechanisms are entirely masked for a dense crystal by the dipolar 'magnon' decoherence, except at high fields (where dipolar decoherence competes with phonon decoherence) or at very low temperatures and low fields (where it competes with nuclear spin decoherence). In this experiment, we chose to go to high fields.

With all this in mind, we return to the ESR results obtained by echo-detected field sweep, in Fig. 1. The resonant peaks are broadened, with a width ~0.1 T; the peculiar structure of the peak when $\mathbf{H}_\perp \| \hat{y}$, discussed in detail in Supplementary Information, comes from dipolar interactions. These ESR signals may be understood as follows. The qubit splitting $2\Delta_o$ varies with field as shown in Fig. 1b inset. For fields $H_y = 9.5$ T, $H_x = 0$, or $H_x = 11.3$ T, $H_y = 0$, the electronic spin Hamiltonian[18,30] for $Fe_8$ predicts $2\Delta_o(\mathbf{H}_\perp) \approx 11.5$ K, equivalent to our spectrometer frequency of 240 GHz (see Fig. 1 inset), implying we should see resonance peaks at these fields. These predictions are reasonably well satisfied in both samples. The discrepancies, discussed in detail in Supplementary Information, come from two sources: (1) sample misorientation, and (2) weak departures at high field from the model Hamiltonian[18,30] used to predict the field splitting.

The results of the measurements for each sample, together with the calculated theoretical decoherence times for $Fe_8$, are presented in Fig. 3. The agreement is very good; we emphasize that apart from the size of the spin–phonon coupling, which is not known exactly, there are no adjustable parameters in these fits. The decoherence times and rates in the experiment range over roughly an order of magnitude, with a maximum $T_2 \approx 0.63$ μs, corresponding to $Q_\phi \approx 1.49 \times 10^6$, at the lowest temperature we went to.

A number of features should be stressed here. First, notice how differently the decoherence and the ESR lineshape are affected by

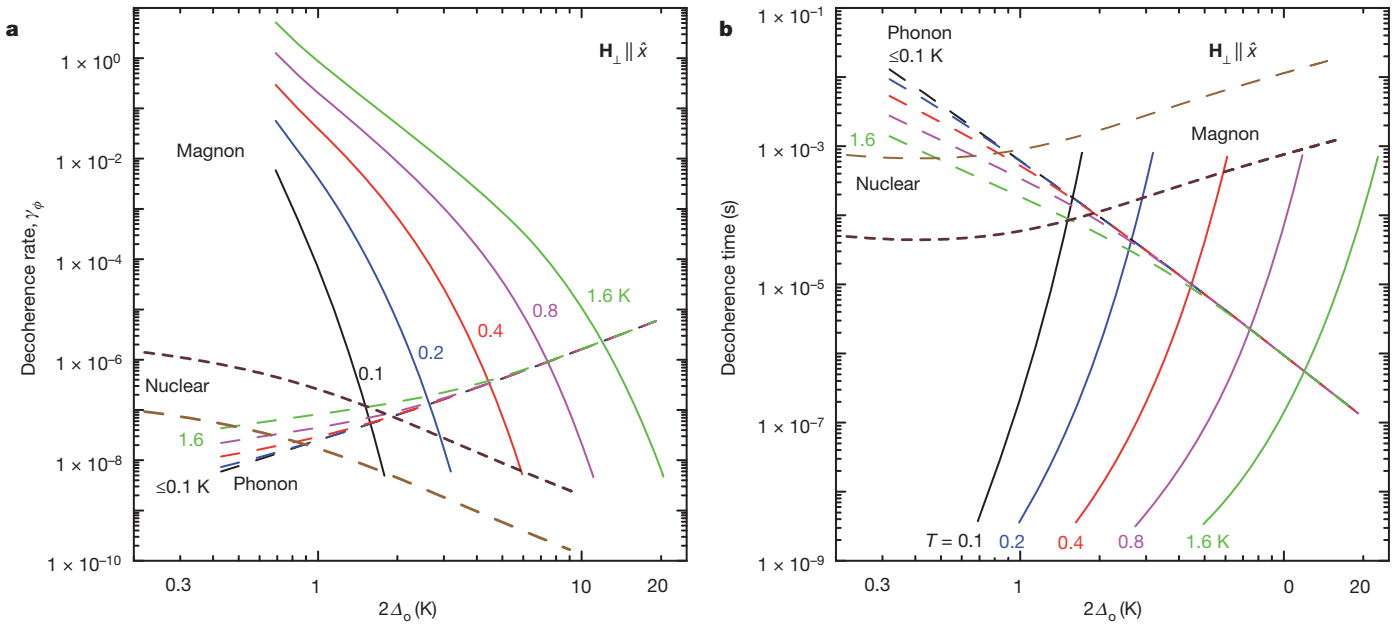


**Figure 2 | Calculated contributions to the decoherence coming from the coupling to nuclear spins, phonons and magnons.** **a**, The three individual contributions which sum to give the dimensionless decoherence rate $\gamma_\phi = \hbar/T_2\Delta_o$, as a function of the qubit splitting in the case $\mathbf{H}_\perp \| \hat{x}$. **b**, The three corresponding contributions to the decoherence time, $T_2$. In both panels: brown dashed lines, nuclear contribution (short-dashed brown lines are for the natural isotopic concentrations, long-dashed brown lines for the deuterated system); solid lines of different colours, magnon contributions at different temperatures (shown) from 0.1 to 1.6 K; long-dashed lines of different colours, phonon contributions, shown for the same temperatures as in the magnon case.

the different environmental couplings. The ESR linewidth and lineshape are completely dominated by static impurity fields and by the spatially varying dipolar fields. However the decoherence is completely dominated, at these high fields, by the phonons and dipolar interactions. At lower fields, the nuclear spin decoherence would also be important, but its effect on the ESR linewidth would still be negligible. Note also that whereas the dipolar contribution to the ESR lineshape depends strongly on sample shape, this shape can only affect the dipolar decoherence near the edges of this line. In the middle of the line, when the decoherence is coming from molecules near the centre of the sample where the field is homogeneous, one expects no dependence of the dipolar decoherence on sample shape. This is also what we found in the experiment.

Second, we emphasize how the experiment tests the phonon and dipolar contributions to the decoherence separately: they have very different temperature dependences in the regime covered here, with

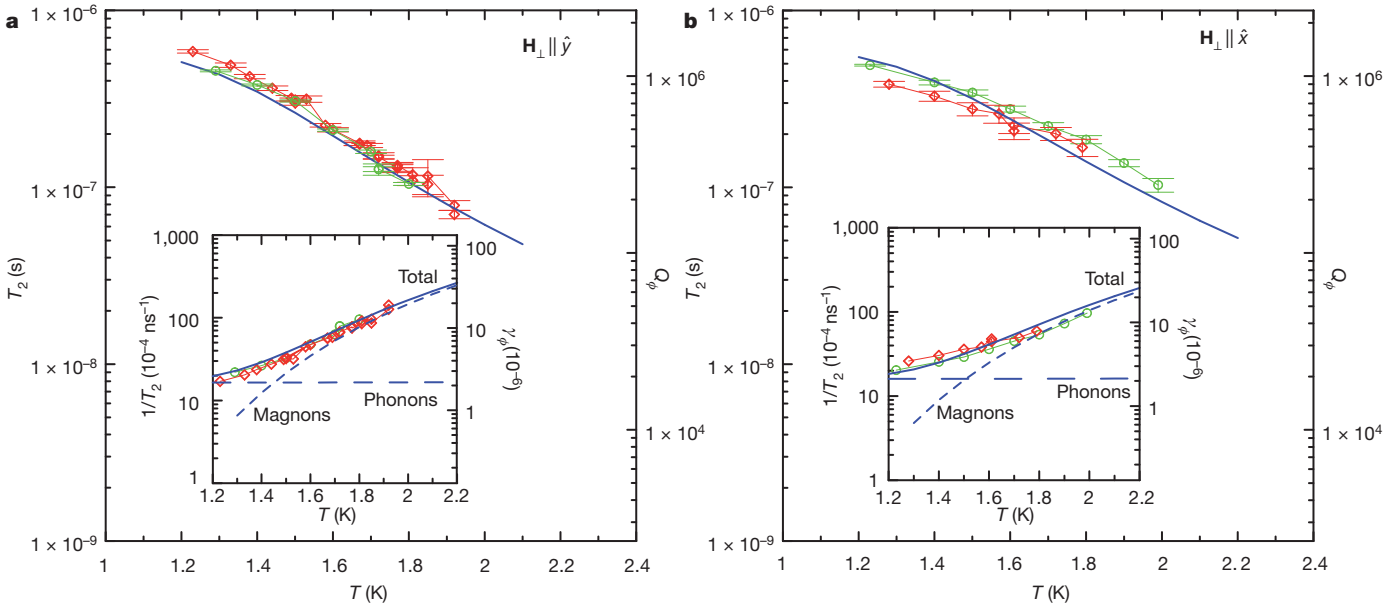


**Figure 3 | Measured and calculated decoherence times $T_2$ in samples 1 and 2, as a function of temperature.** **a**, Results for $\mathbf{H}_\perp \| \hat{y}$. Main panel: thin red line with diamonds, measured using sample 1, $H_y = 9.845$ T; thin green line with circles, measured using sample 2, $H_y = 9.875$ T; vertical and horizontal error bars, standard errors of $T_2$ data fits and uncertainty in temperature ($\Delta T = \pm 0.05$ K), respectively. Thick blue line, calculations including phonon and magnon contributions, $H_y = 9.5$ T. Inset: partial contributions calculated for $T_2^{-1}$ (solid line) from magnons (dashed line) and phonons (long-dashed line), together with the corresponding experimental results for the two samples (diamonds and circles). The scale on the right-hand side of the main panel indicates the decoherence $Q$-factor, $Q_\phi = \pi/\gamma_\phi = \pi T_2 \Delta_o/\hbar$; the right-hand scale on the inset shows $\gamma_\phi$. **b**, As for **a**, but now for $\mathbf{H}_\perp \| \hat{x}$. The experimental curves were measured at $H_x = 10.865$ T (sample 1) and $H_x = 11.953$ T (sample 2). The theoretical curves are obtained at $H_x = 11.3$ T.

phonons dominating below ~1.2 K, and magnons dominating at higher temperature. We find agreement between theory and experiment, with no adjustable parameters, across roughly an order of magnitude in decoherence rate. Thus all decoherence in the experiment can be accounted for by environmental sources. This implies that we have no measurable extrinsic decoherence here, either from disorder or dynamic impurities. Nor do we have evidence for any other contributions, either from "third-party decoherence"[4], or from any of the 'intrinsic decoherence' sources[1] discussed in the literature.

Third, we note a key difference between the coherence here, which involves a macroscopic number of qubits excited coherently in a spin wave, and that in other qubit systems, in which entanglement is achieved locally, involving just one or a few qubits. The reason we can do this is because we are dealing with a single crystal.

Last, the present investigation suggests that one can optimize the qubit decoherence $T_2$ and $Q$-factor $Q_\phi$, as a function of field and temperature, using the results plotted in Fig. 2. We see that lower temperature allows use of a smaller ESR frequency $2\Delta_o$; these two changes strongly reduce the dipolar and phonon decoherence contributions, giving a large increase in $T_2$, and a somewhat smaller increase in $Q_\phi$. The optimal decoherence rate comes when the phonon and nuclear spin decoherence contributions cross (for natural isotopic concentrations, this is at $2\Delta_o \approx 2$ K), provided also that $T < 0.13$ K, so that the dipolar/magnon decoherence can be ignored. One then finds that $\gamma_\phi \approx 1.5 \times 10^{-7}$, so that $Q_\phi = 2 \times 10^7$, corresponding to a decoherence time $T_2 \approx 50\,\mu$s. However with isotopic substitution of deuterons in place of the protons, the optimal decoherence time rises to $T_2 \approx 500\,\mu$s, at $2\Delta_o = 0.8\,\text{K} \equiv 17$ GHz, and $T = 45$ mK. This corresponds to $\gamma_\phi \approx 5 \times 10^{-8}$ and $Q_\phi \approx 6 \times 10^7$. These considerations show the usefulness of this kind of theory in the optimal design of spin qubit systems––notice the crucial importance of controlling the dipolar interactions between qubits. Notice also that if quantum mechanics is to be tested on anything but microscopic scales, it will be essential to continue developing theory and experiment for systems like the present one, where the environmental decoherence processes can be understood quantitatively, and where extrinsic decoherence sources can be largely eliminated.

## METHODS SUMMARY

The single molecule characteristics were calculated using previous results for crystal field parameters[30] and for the effect of high field on these[18]. Hyperfine couplings were taken from previous work[18]; the spin–phonon couplings were estimated using standard magnetostriction theory, in the high field regime. The dipolar fields were calculated numerically, taking into account the unit cell crystal structure, the sample shape and the field direction, for each sample. The nuclear spin and phonon decoherence rates were determined analytically, using standard methods[16,17], using the previously determined hyperfine and spin–phonon couplings. The dipolar decoherence rate, from four-magnon scattering and decay processes, was determined numerically, for the given sample shape, field and crystal lattice structure, using analytic formulas[18] for the magnon spectrum and dipolar coupling functions.

Single crystals of $Fe_8$ magnetic molecules were synthesized using the method of ref. 19. Each crystal was indexed and unit-cell parameters were checked to ensure consistency. Continuous-wave/pulsed ESR measurements were carried out using the 240-GHz ESR spectrometer at the National High Magnetic Field Laboratory (NHMFL)[21,22]. The system consists of a 12.5-T superconducting magnet, a 40-mW 240-GHz source, quasioptics, a superheterodyne detection system, and a $^4$He flow cryostat. The spin decoherence time was measured by a Hahn echo sequence ($\pi/2$-$\tau$-$\pi$-$\tau$-echo) where the delay $\tau$ is varied[20]. The magnetic component of the 240-GHz pulses was perpendicular to the d.c. magnetic field, to generate coherent magnons in the sample; their duration was adjusted to maximize the echo signals, and was typically 200–300 ns.

**Received 3 April; accepted 16 June 2011.**
**Published online 20 July 2011.**

1. 't Hooft, G. Quantum gravity as a dissipative deterministic system. *Class. Quantum Gravity* **16,** 3263–3279 (1999).
2. Penrose, R. On gravity's role in quantum state reduction. *Gen. Relativ. Gravit.* **28,** 581–600 (1996).
3. Leggett, A. J. Testing the limits of quantum mechanics: motivation, state of play, prospects. *J. Phys. Condens. Matter* **14,** R415–R451 (2002).
4. Stamp, P. C. E. The decoherence puzzle. *Stud. Hist. Phil. Mod. Phys.* **37,** 467–497 (2006).
5. Gatteschi, D., Sessoli, R. & Villain, J. *Molecular Nanomagnets* (Oxford Univ. Press, 2006).
6. Takahashi, S. *et al.* Coherent manipulation and decoherence of S = 10 single-molecule magnets. *Phys. Rev. Lett.* **102,** 087603 (2009).
7. Bertaina, S. *et al.* Quantum oscillations in a molecular magnet. *Nature* **453,** 203–206 (2008).
8. Schlegel, C. *et al.* Direct observation of quantum coherence in single-molecule magnets. *Phys. Rev. Lett.* **101,** 147203 (2008).
9. Leibfried, D., Blatt, R., Monroe, C. & Wineland, D. Quantum dynamics of single trapped ions. *Rev. Mod. Phys.* **75,** 281–324 (2003).
10. Labaziewicz, J. *et al.* Temperature dependence of electric field noise above gold surfaces. *Phys. Rev. Lett.* **101,** 180602 (2008).
11. Xu, X. *et al.* Optically controlled locking of the nuclear field via coherent dark-state spectroscopy. *Nature* **459,** 1105–1109 (2009).
12. Ladd, T. D. *et al.* Pulsed nuclear pumping and spin diffusion in a single charged quantum dot. *Phys. Rev. Lett.* **105,** 107401 (2010).
13. Takahashi, S. *et al.* Quenching spin decoherence in diamond through spin bath polarization. *Phys. Rev. Lett.* **101,** 047601 (2008).
14. Childress, L. *et al.* Coherent dynamics of coupled electron and nuclear spin qubits in diamond. *Science* **314,** 281–285 (2006).
15. Hanson, R. *et al.* Coherent dynamics of a single spin interacting with an adjustable spin bath. *Science* **320,** 352–355 (2008).
16. Leggett, A. J. *et al.* Dynamics of the dissipative two-state system. *Rev. Mod. Phys.* **59,** 1–85 (1987).
17. Prokof'ev, N. V. & Stamp, P. C. E. Theory of the spin bath. *Rep. Prog. Phys.* **63,** 669–726 (2000).
18. Morello, A., Stamp, P. C. E. & Tupitsyn, I. S. Pairwise decoherence in coupled spin qubit networks. *Phys. Rev. Lett.* **97,** 207206 (2006).
19. Wieghardt, K., Pohl, K., Jibril, I. & Huttner, G. Hydrolysis products of the monomeric amine complex $(C_6H_{15}N_3)FeCl_3$: the structure of the octameric iron(III) cation of $[(C_6H_{15}N_3)_6Fe_8(\mu 3\text{–}O)_2(\mu_2\text{–}OH)_{12}]Br_7 \cdot 8H_2O$. *Angew. Chem. Int. Edn Engl.* **23,** 77–78 (1984).
20. Hahn, E. L. Spin echoes. *Phys. Rev.* **80,** 580–594 (1950).
21. van Tol, J., Brunel, L. C. & Wylde, R. J. A quasioptical transient electron spin resonance spectrometer operating at 120 and 240 GHz. *Rev. Sci. Instrum.* **76,** 074101 (2005).
22. Morley, G. W., Brunel, L. C. & van Tol, J. A multifrequency high-field pulsed electron paramagnetic resonance/electron-nuclear double resonance spectrometer. *Rev. Sci. Instrum.* **79,** 064703 (2008).
23. Stamp, P. C. E. & Tupitsyn, I. S. Coherence window in the dynamics of quantum nanomagnets. *Phys. Rev. B* **69,** 014401 (2004).
24. Yao, W., Liu, R. B. & Sham, L. J. Theory of electron spin decoherence by interacting spins in a quantum dot. *Phys. Rev. B* **74,** 195301 (2006).
25. Morello, A., Bakharev, O. N., Brom, H. B., Sessoli, R. & de Jongh, L. J. Nuclear Spin Dynamics in the Quantum regime of a single molecule magnet. *Phys. Rev. Lett.* **93,** 197202 (2004).
26. Cuccoli, A. *et al.* Dipolar interaction and incoherent quantum tunneling: a Monte Carlo study of magnetic relaxation. *Europhys. J. B.* **12,** 39–46 (1999).
27. Tupitsyn, I. S., Stamp, P. C. E. & Prokofev, N. V. Hole digging in ensembles of tunneling molecular magnets. *Phys. Rev. B* **69,** 132406 (2004).
28. Hill, S. *et al.* D-strain, g-strain, and dipolar interactions in the $Fe_8$ and $Mn_{12}$ single molecule magnets: an EPR lineshape analysis. *Int. J. Mod. Phys. B* **16,** 3326–3329 (2002).
29. Park, K. *et al.* Effects of D-strain, g-strain, and dipolar interactions on EPR linewidths of the molecular magnets $Fe_8$ and $Mn_{12}$. *Phys. Rev. B* **65,** 014426 (2001).
30. Barra, A. L., Gatteschi, D. & Sessoli, R. High-frequency EPR spectra of $[Fe_8O_2(OH)_{12}(tacn)_6]Br_8$: a critical appraisal of the barrier for the reorientation of the magnetization in single-molecule magnets. *Chem. Eur. J.* **6,** 1608–1614 (2000).

**Supplementary Information** is linked to the online version of the paper at www.nature.com/nature.

**Acknowledgements** This work was supported by the NSF (DMR-0520481, DMR-0703925), the Keck Foundation (S.T. and J.v.T.), NSERC, CIFAR, PITP, the John E. Fetzer Memorial Trust (grant D21-C62) and the Center for Philosophy and the Natural Sciences, California State University, Sacramento (I.S.T. and P.C.E.S.). The National High Magnetic Field Laboratory is supported by NSF Cooperative Agreement DMR-0654118, by the State of Florida, and by the DOE.

**Author Contributions** S.T., I.S.T. and P.C.E.S. contributed to the writing of the manuscript. S.T., I.S.T. and P.C.E.S. conceived the ESR experiments. The ESR measurements were carried out by S.T. and J.v.T. The theoretical work was done by I.S.T. and P.C.E.S. C.C.B and D.N.H. synthesized $Fe_8$ crystals and performed X-ray diffraction measurements.

**Author Information** Reprints and permissions information is available at www.nature.com/reprints. The authors declare no competing financial interests. Readers are welcome to comment on the online version of this article at www.nature.com/nature. Correspondence and requests for materials should be addressed to S.T. (susumuta@usc.edu) or P.C.E.S. (stamp@phas.ubc.ca).